Printed ISSN 1330–0016
Online ISSN 1333–9133
CD ISSN 1333–8390
CODEN FIZBE7

INVESTIGATION OF DIPOLE EXCITATIONS BELOW THE GIANT DIPOLE RESONANCE IN ^{89}Y USING THE ELBE FACILITY

N. BENOUARET[a,b], R. SCHWENGNER[b], G. RUSEV[b,d], F. DÖNAU[b], R. BEYER[b], M. ERHARD[b], E. GROSSE[b,c], A. R. JUNGHANS[b], K. KOSEV[b], C. NAIR[b], K. D. SCHILLING[b] and A. WAGNER[b]

[a]*Faculté de physique, Université des Sciences et de la Technologie d'Alger, Algerie*

[b]*Institut für Strahlenphysik, Helmholtz-Zentrum Dresden-Rossendorf, Dresden, Germany*

[c]*Institut für Kern-und Teilchenphysik, Technische Universität Dresden, Dresden, Germany*

[d]*Present address: Department of Physics, Duke University, Triangle Universities Nuclear Laboratory, Durham, NC 27708, U. S. A.*

Received 20 December 2010; Accepted 14 December 2011
Online 3 February 2012

We have investigated the dipole response of the stable $N = 50$ nucleus ^{89}Y up to the excitation energy of the giant dipole resonance (GDR) using the bremsstrahlung facility at the ELBE accelerator at the research center Helmholtz-Zentrum Dresden-Rossendorf. After eliminating background radiation from atomic processes as well as inelastic transitions in the spectra by using statistical methods, the photoabsorption cross section could be deduced from the photon-scattering data. This cross section was combined with that known from (γ, n) experiments. An excess of the cross section relative to a simple Lorentz approximation of the tail of the GDR is found in the energy range from about 6 MeV up to 11 MeV. The comparison with predictions of a quasiparticle-random-phase approximation (QRPA) showed that the corresponding excitations may be caused by an oscillation of the excessive neutrons forming a so-called pygmy dipole resonance (PDR) as it was found for the neighbouring isotones ^{88}Sr and ^{90}Zr.

PACS numbers: 25.20.Dc, 23.20.-g UDC 539.143, 539.166

Keywords: photon scattering, dipole resonances in ^{89}Y, up to giant dipole resonance, quasiparticle-random-phase approximation, pygmy dipole resonances

1. Introduction

The lowest-lying excited states of magic and semimagic nuclei are known to be a $J^\pi = 2_1^+$ quadrupole vibration and a $J^\pi = 3_1^-$ octupole vibration of the nuclei. The collective character is indicated by transitions probabilities larger than 10 W.u.

Electric dipole excitations observed close to the sum of the energies of the 2^+ and 3^- states ($B(E1) \approx$ mW.u.) were associated to the $J = 1^-$ member of the $\left(2_1^+ \otimes 3_1^-\right)$ multiplet [1]. The dynamic octupole shape of the $J^\pi = 3_1^-$ is responsible for the generated electric dipole moment in the 1^- state [2, 3].

At higher excitation energy, around $10-15$ MeV, the electric dipole giant resonance (≈ 10 W.u. appears which consists of a coherent superposition of particle-hole excitations and can be described as an out-of-phase oscillation of the neutron versus the proton fluid.

In the last decade, the advent of the new generation of germanium detector with a better resolution and efficiency and using high photon flux in photon scattering experiments, the research has focused on the energy region located just below the giant dipole excitation energy of closed shell nuclei. Surprisingly, this region revealed a concentration of electric dipole transitions ($\approx 10^{-3}$ W.u.), suggesting a new mode of excitation called Pygmy dipole resonance (PDR) to distinguish it from the GDR. It was reported in the closed-shell $Z = 82$, $N = 126$ nucleus ^{208}Pb [4, 5], the $N = 82$ nuclei ^{136}Xe,^{136}Ba, ^{140}Ce, ^{142}Nd and ^{144}Sm [6 − 9] and in the $Z = 20$ nuclei ^{40,44,48}Ca [10]. It was noted that this enhancement was connected to the N/Z ratio.

The structure of the corresponding states was studied within many theoretical models using microscopic or macroscopic approaches, such as the twofluid hydrodynamical model [11], the density functionnel theory [12], the Hartree-Fock plus random phase approximation (RPA) with Fritz skyrme forces [13], the quasi-particle random phase approximation plus phonon coupling [14], the relativistic RPA [15], the relativistic QRPA [16] and the quasiparticle phonon model (QPM) [17]. The QPM describes the excitation of PDR states as associated to an out-of-phase oscillation of a neutron skin against the $N \approx Z$ core.

The nature and systematic features, such as the dependence of the centroid energy, the width and the dependence of the strength of the PDR on the N/Z ratio in each chain remain under discussion.

Strong dipole excitations were also observed in exotic nuclei very rich with neutrons [18, 19]. Consequently, it is interesting to look if it corresponds to the same phenomenon as in the nuclei in and close to the valley of stability. Moreover, the data of (γ, n) reactions at energies lower than the GDR are important to calculate the abundances of heavy nuclei in stars [20].

Enhanced strength with respect to simple extrapolations of the GDR by Lorentz functions and the relation of this strength to a PDR have recently been studied in the $N = 50$ closed-shell nuclei ^{92}Mo [21], ^{88}Sr [22] and ^{90}Zr [23]. For the first time, strength in the quasi-continuum has been taken into account and the intensities of inelastic transitions have been estimated. The present work reports on NRF experiments on the odd-proton isotone ^{89}Y [24].

2. Experimental method

2.1. Nuclear resonance fluorescence technique

The nuclear resonance fluorescence experiments (NRF) [25, 26] are well suited to investigate dipole excitations of the nucleus due to the low transfer of angular momentum of the bremsstrahlung photons. Moreover, due to the corresponding continuous energy, all levels are simultaniously populated.

The scattering cross section I_S integrated over the energy width of a resolved resonance associated to an excited level E_x is calculated from the measured transition intensity de-exciting this level to the ground state (the detector resolution $\Delta E \approx 7$ keV at 9 MeV is much greater than the natural level width).

The integrated scattering cross section I_S is connected to the partial level width Γ_0 of de-excitation of the photo-excited level with spin J and excitation energy E_x from the ground-state level with spin J_0 according to

$$I_S = \int \sigma_{\gamma\gamma} \mathrm{d}E = \frac{2J+1}{2J_0+1} \left(\frac{\pi\hbar c}{E_x}\right)^2 \frac{\Gamma_0^2}{\Gamma}\,, \tag{1}$$

where $\sigma_{\gamma\gamma}$ is the elastic scattering cross section and Γ is the total level width.

By measuring I_S, following Eq. (1), the ground state partial width times the branching ratio Γ_0^2/Γ can be then extracted.

2.2. Experimental setup

Two experiments on the ^{89}Y nucleus were performed at the bremsstrahlung facility at the superconducting electron accelerator ELBE of the research center Dresden-Rossendorf [27] (Fig. 1) with electron beams of 9.5 MeV and 13.2 MeV kinetic energy and average currents of 520 and 600 μA, respectively. The corresponding bremsstrahlung beams were produced by electron beams hitting 4 and 7 μm thick niobium foils. An aluminium attenuator of 10 cm thickness was placed behind the radiator to reduce the low-energy part of the bremsstrahlung spectrum.

The photon beam is collimated on the 20 mm target to a spot of 38 mm diameter giving an uniform photon flux ($\approx 10^9$ s^{-1}). 3303.2 mg of natural yttrium powder was sandwiched with a disk of 20 mm in diameter of 339.5 mg of ^{11}B enriched to 99.52% which was used for measuring the photon flux. The irradiation time of the two experiments was 78 h and 87 h, respectively.

The scattered photons were detected by four HPGe (high-purity germanium) detectors with efficiencies of about 100% relative to a NaI detector (a cylinder with a length of 3 in. and a diameter of 3 in.). Two HPGe detectors were placed at a distance of 28 cm from the target under $\theta = 90^\circ$ and another two at a distance of 32 cm under 127° relatively to the incident photon beam. Low-energy photons from the target were suppressed by absorbers placed at the front face of each detector: 13mm thick lead and 3 mm thick copper on detectors located at 90° and 8 mm thick

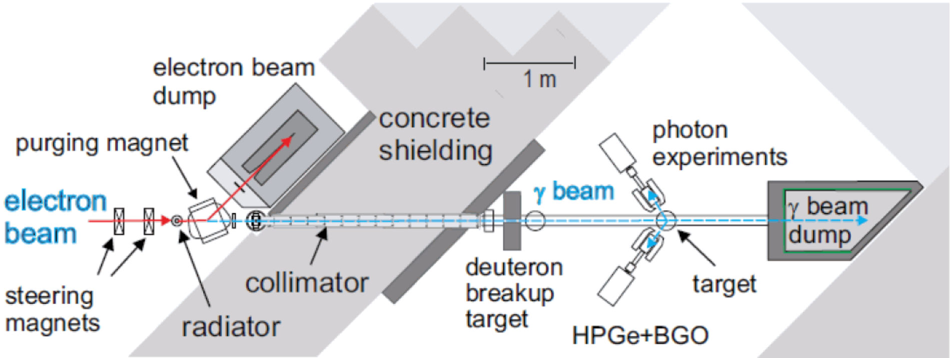

Fig. 1. Schematic view of the NRF setup at ELBE.

lead and 3 mm thick copper on detectors at 127°. All detectors were surrounded by escape-suppression shields made of bismuth germanate scintillation detectors.

The absolute efficiency of the dectectors was determined using ^{60}Co, ^{133}Ba, ^{137}Cs and ^{226}Ra standard calibration sources. The efficiency curve was extrapolated to high energy by simulations using the code GEANT3 [28] (Fig. 2). The reliability was checked by comparison to the efficiencies obtained using ^{11}B transitions [22].

The ^{11}B transitions were also used to calculate the incident photon flux from the corresponding measured intensities of transitions from states with known integrated cross sections. The interpolation was performed [22] using a curve calculated with the code described in Ref. [29].

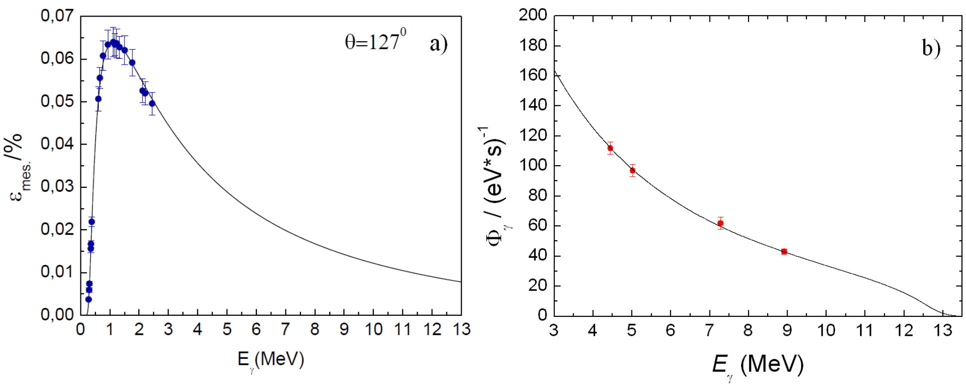

Fig. 2. a) Absolute efficiency values of the two detectors at 127° determined from standard calibration sources (dots) and efficiency calculated with GEANT3 (solid line). b) Absolute photon flux deduced from transitions in ^{11}B (dots) and calculated photon flux (solid line).

3. *Experimental results*

Figure 3 shows parts of the obtained spectra corrected for energy efficiency measured at 9.5 MeV and 13.2 MeV at the angle of 127°.

The spectrum consists of resolved transitions and unresolved weak transitions which form a continuum. The continiuum is a consequence of the high level density at high excitation energy.

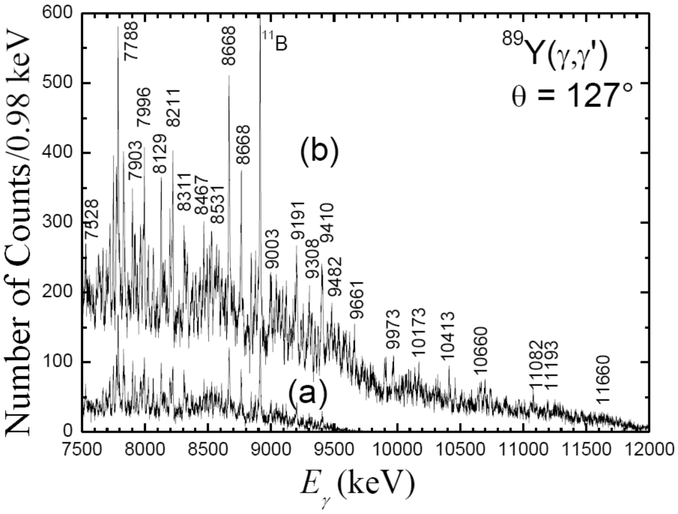

Fig. 3. NRF spectra corrected for detection efficiency at electron energies of a) 9.5 MeV *and b) 13.2* MeV.

3.1. *Resolved transitions*

The resolved transitions are originating from deexcitation of photoexcited levels to the ground state (elastic transitions) as well as to the low lying states (inelastic transitions). To determine the integrated elastic scattering cross section, spectra with electron kinetic energies of 9.5 and 13.2 MeV have been compared. Elastic transitions already identified by Reif et al. [30] in the NRF experiment at 7 MeV have also been taken into account. Thus, all transitions observed up to 7 MeV energy in the spectra measured at 9.5 and 13.2 MeV, but not listed by Reif et al., are considered inelastic. Similarly, all transitions to the energy 9.5 MeV observed only in the spectra measured at 13.2 MeV transitions are considered inelastic deexcitation of the levels located above 9.5 MeV.

The integrated elastic scattering cross section I_S associated to the deexcitation of a level at E_x with a ground state transition E_γ was deduced relative to the one known for a transition in ^{11}B,

$$I_S(E_x) = I_S(E_x^B)\,\frac{I_\gamma(E_\gamma,\theta)}{I_\gamma(E_\gamma^B,\theta)}\,\frac{W(E_\gamma^B,\theta)}{W(E_\gamma,\theta)}\,\frac{N_N^B}{N_N}\,\frac{\phi_\gamma(E_x^B)}{\phi_\gamma(E_x)}\,, \tag{2}$$

where $I_\gamma(E_\gamma, \theta)$ and $I_\gamma(E_\gamma^B, \theta)$ are the intensities of ground state transitions E_γ in ^{89}Y and E_γ^B of ^{11}B, detected under the angle θ relative to the beam. The quantities $W(E_\gamma^B, \theta)$ and $W(E_\gamma, \theta)$ represent the corresponding angular correlations. N_N and N_N^B are the numbers of nuclei in ^{89}Y and in ^{11}B targets, respectively. $\phi_\gamma(E_x^B)/\phi_\gamma(E_x)$ is the ratio of the photon flux at the energy of the ground-state transition to a level at E_x^B in ^{11}B to the one at the energy of the considered transition.

However, a level can be excited at the same time directly by an incident bremstrahlung photon or by the levels situated above (feeding). Therefore, it is necessary to estimate the influence of the feeding intensity on the elastic transition intensity. Figure 4 shows the ratios of the integrated scattering cross section I_{S+f} including the feeding and deduced from the observed intensity at different electron energies.

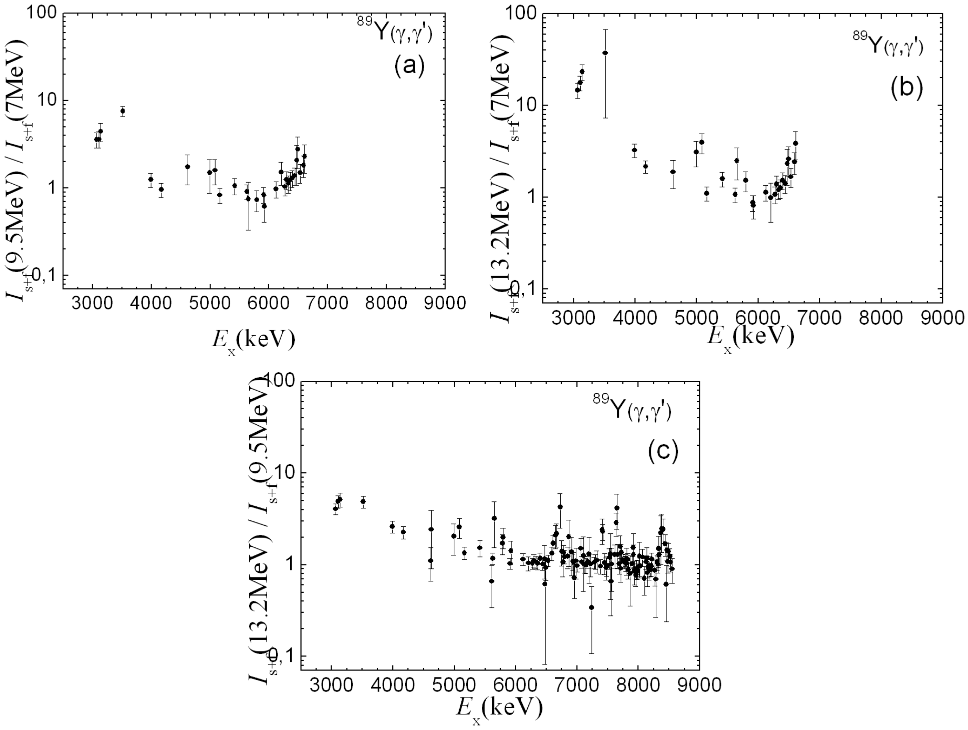

Fig. 4. Ratios of integrated cross section I_{s+f} of ^{89}Y obtained at different electron energies.

The ratios show that levels situated at excitation energies below 6 MeV are significantly influenced by feeding (values differing from unity), mainly due to energy levels located above 9 MeV. The large ratios calculated using the cross sections of Reif et al. [30] could indicate a systematic experimental uncertainty due to an overestimate of the photon flux in the vicinity of the maximum energy of the bremsstrahlung spectrum.

The ^{89}Y photo-excited energy levels were determined from the transitions considered as transitions to the ground state. Most of the intensity ratios $I_\gamma(90°)/I_\gamma(127°)$ were too uncertain to distinguish between the corresponding theoretical values (0.87 for a pure dipole transition and 1.15 for a quadrupole transition). Hence, no spin assignment was possible. Therefore, only the strength distribution represented by the quantity $g\Gamma_0^2/\Gamma$, the product of the partial width for the ground state and the branching ratio, multiplied by the the statistical factor g, could be deduced from the measured integrated cross section [24] (Fig. 5).

By analogy with the neighbouring isotones ^{88}Sr [22] and ^{90}Zr [23], the transitions with energy higher than 6 MeV in ^{89}Y were considered as dipole transitions.

The detection limit, defined as twice the statistical uncertainty of the area of a background window with a length corresponding to the full width at half maximum of a peak at the same energy, is shown in Fig. 6 in terms of reduced partial width times the branching ratio $g\Gamma_0^2/(\Gamma E_\gamma^3)$.

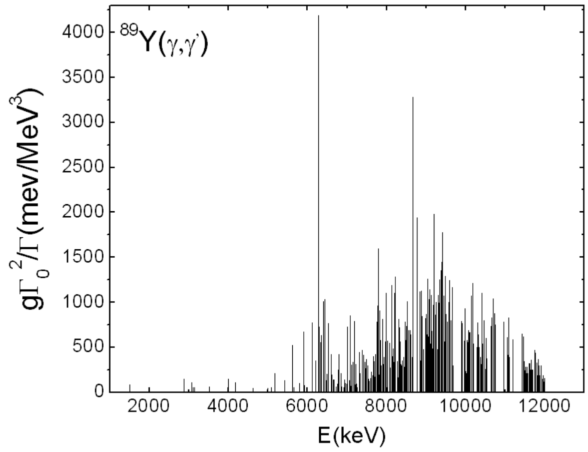

Fig. 5. Distribution of resolved strength of ^{89}Y *up to GDR excitation energy.*

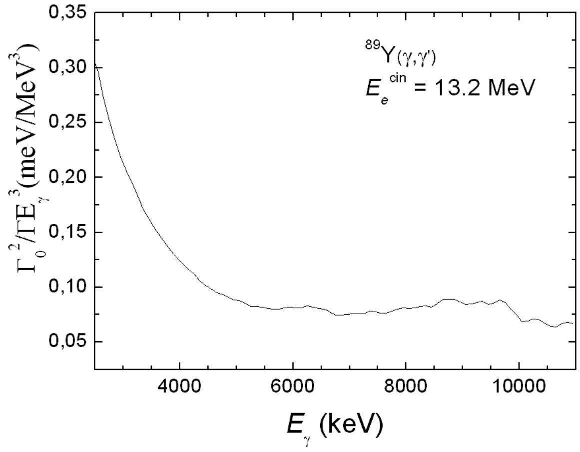

Fig. 6. Detection limit for resolved transitions in the measurement at 13.2 MeV.

3.2. Unresolved transitions – statistical analysis

In order to restitute the intensity from the continuum and to correct it by the branching transition intensity, simulations of γ-ray cascades were performed [20].

3.2.1. Background atomic process and detector response substraction

As a first step, after subtracting the ambient background, the experimental spectrum was corrected for the background produced from atomic processes in HP(Ge) detectors and in the target using GEANT3 simulations and using the absolute photon flux obtained from ^{11}B transitions. Intensity contributions originating from (γn) reactions in HP(Ge) detectors and in surrounding materials were negligible.

As can be seen in Fig. 7, *the contribution of continuum* intensity in the spectrum corrected by detector response is clearly visible above *the atomic background*.

The scattering cross sections $\sigma_{\gamma\gamma}$, derived from the intensity obtained from resolved peaks as well as unresolved peaks shown in Fig. 8 are by a factor of about 4 greater than the ones accounting on only the resolved peak intensity. Moreover, both corresponding distributions show similar structures caused by the prominent peaks. This is a second indication of the existing continuum.

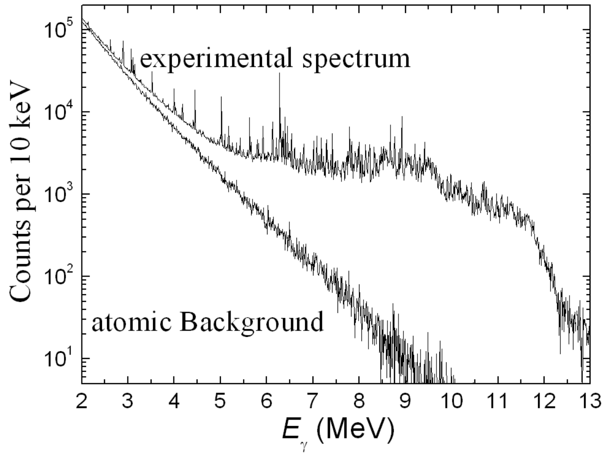

Fig. 7. ^{89}Y *Experimental spectrum measured at 13.2* MeV *corrected for room background and detector response and simulated atomic background.*

3.2.2. Simulations of gamma ray cascades

In order to correct the intensity of the ground state transitions by removing the intensities of branching transitions of each level and therefore to deduce the ground state transition intensity, simulations of 1000 level schemes (nuclear realizations) were performed starting from the ground state.

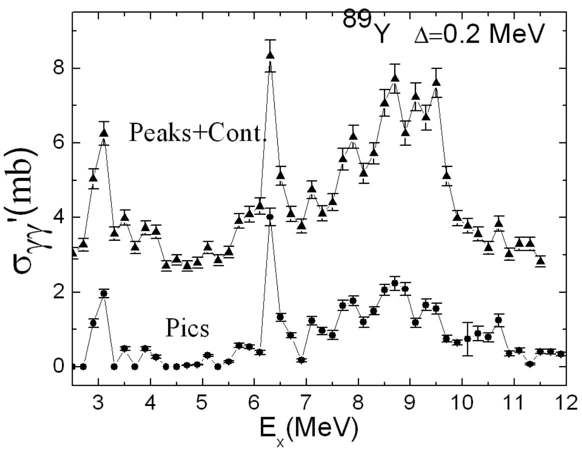

Fig. 8. ^{89}Y scattering cross sections derived from the total intensity of peaks and continuum in an energy bin Δ and compared to the peak intensity only in the same bin.

The level density is given by the backshifted Fermi gas model (BSFG) with parameters $a = 9.39(16)$ MeV^{-1} and $E_1 = 0.32(6)$ MeV, obtained from empirical formulas based on fits to experimental level densities [31]. The same level densities are assumed for states with positive parities and negative parities. The energy spacings follow a Wigner distribution [32], and a distribution of Porter-Thomas is used for the fluctuations of the partial widths [33]. The level density calculated for levels with spin $J = 3/2$ is compared to the one derived from the resolved transitions in Fig. 9. The discrepancy is seen again with a remarkable portion of unresolved transitions in the continuum.

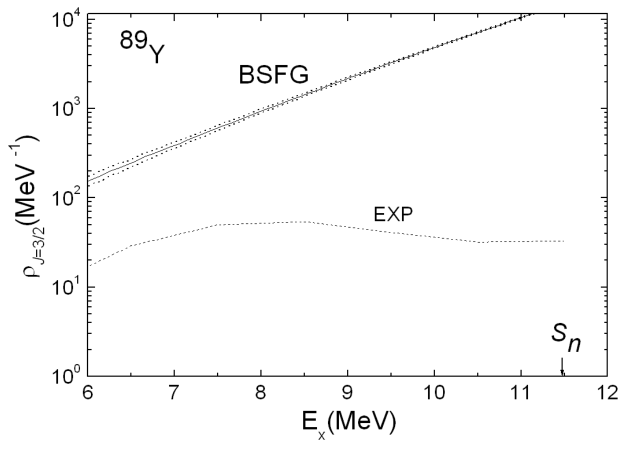

Fig. 9. Level densities of $J = 3/2$ states as a function of excitation energy resulting from BSFG model and from the experimental levels.

Lorentz parametrizations [34] were used for the E1, M1 and E2 photon strength functions. The parameters of the lorentzian for the E1 strength were taken from a fit to the (γ, n) data [35]. The parameters for the M1 and E2 strengths were taken from global parametrizations of M1 spin-flip resonances and E2 isoscalair resonances, respectively.

Once the 1000 level schemes have been created, considering levels in 0.1 MeV bins in each level scheme and starting from the high-energy end of the experimental spectrum, which contains ground-state transitions only, the simulated intensities of the ground state transitions were scaled to the experimental ones in the considered energy bin and the intensity distribution of the branching transitions was subtracted from the experimental spectrum. Applying this procedure step by step for each energy bin, moving toward the low energy end of the spectrum, one obtains the intensity distribution of the ground-state transitions. Simultaneously, the ground state branching ratio b_0^{Δ} is calculated as the ratio of the sum of intensities of the ground state transitions from all levels in Δ to the total intensity of all transitions depopulating those levels to any low-lying levels including the ground state. Figure 10 displays the mean branching ratios calculated using 10 nuclear realizations.

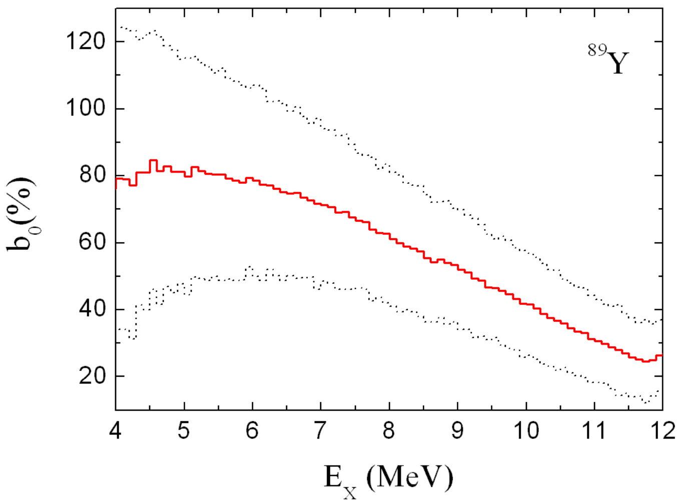

Fig. 10. Ground-state transition branching ratios obtained by averaging values from 10 nuclear realizations (middle line). The lower and upper dotted lines correspond to the minimum and maximum branching ratio values.

In this figure we can see that the branching ratio decreases from 80% at about 5 MeV, where the level density is low and only a few inelastic transitions are possible, to about 40% near the neutron separation energy. This percentage at about 11 MeV is smaller than that found in the neighboring even-even isotones ^{88}Sr [21] and ^{90}Zr [22] which is around 65%. This effect has the consequence of the higher level density in the odd-mass nucleus ^{89}Y due to the multitude ways of coupling of the unpaired proton to the even core.

3.2.3. Corrected photoabsorption cross section

In order to connect our results to the data belonging to the low-energy part of the GDR, the photoabsorption cross section is calculated for each bin averaging over the values of the 1000 nuclear realizations. It is obtained as $\sigma_\gamma^\Delta = \sigma_{\gamma\gamma}^\Delta / b_0^\Delta$, where $\sigma_{\gamma\gamma}^\Delta$ corresponds to the summed ground state transitions intensity in a bin, and b_0^Δ is the corresponding branching ratio. A deviation of $1\,\sigma$ from the mean has been taken for the uncertainty of the absorption cross section.

The corresponding values are plotted in Fig. 11 and compared with those deduced from the uncorrected spectrum.

In Fig. 11, we also show the absorption cross sections of (γ, n) [35] and those of (γ, p) calculations [36]. One sees an enhancement of the strength at high energy which result from the division by the branching ratio.

The total photoabsorption cross section has been deduced by combining the present (γ, γ') *data with the* (γ, n) *data* and with the calculated (γ, p) cross sections. The data were averaged over 0.5 MeV bins to reduce statistical fluctuations. This total cross section is compared with the Lorentz curve obtained from a fit to (γ, n) data (Fig. 12). The comparison shows extra strength relatively to the approximation of the low-energy tail of the GDR by a Lorentz curve in the energy range from 6 to 11 MeV.

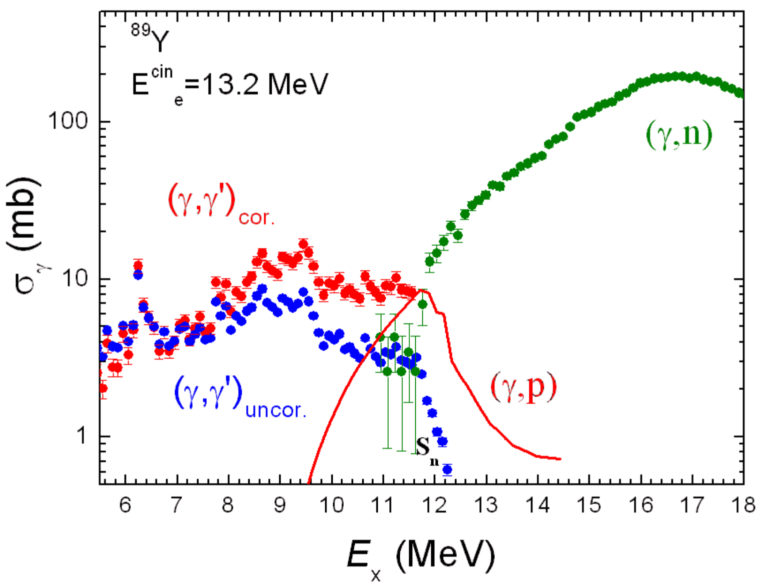

Fig. 11. Uncorrected (black circles) and corrected (red circles) photoabsorption cross sections deduced from the measurement at 13.2 MeV *[24] in comparison with* (γ, n) *data [35] and* (γ, p) *calculations [36].*

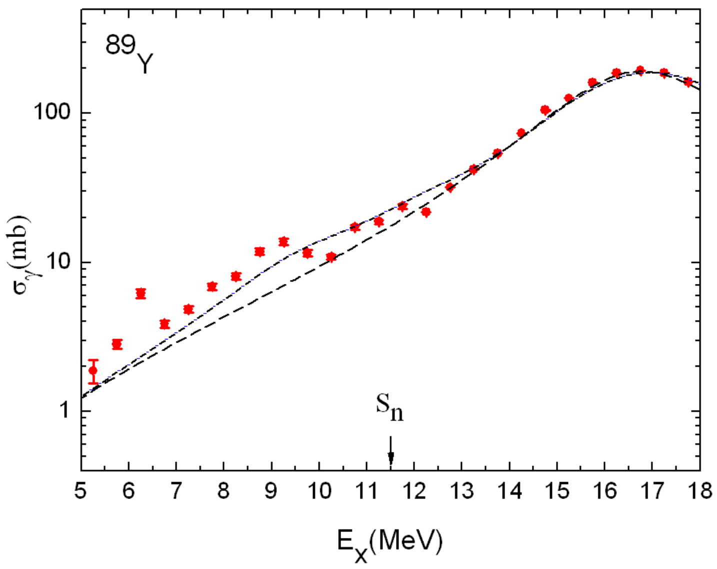

Fig. 12. Total photo absorption cross section (red circles) of ^{89}Y *obtained by combining the present* (γ, γ') *data, the* (γ, n) *data of Ref. [35] and* (γ, p) *calculations of Ref. [36]. The black dashed line represents a Lorentz distribution with the parameters given in the text. The blue dashed line is the result of the QRPA calculations.*

4. Interpretation of the results in the framework of the QRPA model

We have compared the measured ^{89}Y photo absorption cross section to the one calculated by using the QRPA model [37, 38]. In the considered energy region above 5 MeV, the dipole cross section is dominated by the electric (E1) dipole transitions, while possible contributions of magnetic (M1) transitions as well as electric quadrupole (E2) transitions can be neglected.

In the QRPA model, two kinds of residual interaction are included, the first one is of short range (pairing) which is taken into account by the monopole pair field. The second one is of long-range character which is modeled as a separable dipole-dipole plus octupole-octupole interaction .

4.1. QRPA calculations

The nucleus ^{89}Y has a closed $N = 50$ neutron shell which leads to a spherical equilibrium shape of the $J^\pi = 1/2^-$ ground state. The E1 dipole excitation by the photons can generate $J^\pi = 1/2^+$ and $3/2^+$ excited states which can be described by the Hamiltonian

$$H_{E1}^{\mathrm{QRPA}} = h_{\mathrm{ch.moy}}^{(p)} + h_{\mathrm{ch.moy}}^{(n)} - \frac{1}{2}\sum_{t=0,1}\sum_{\mu=-1,1}\chi_{1\mu}^{t} Q_{1\mu}^{t} Q_{1-\mu}^{t} - \frac{1}{2}\sum_{t=0,1}\sum_{\mu=-3,3}\chi_{3\mu}^{t} Q_{3\mu}^{t} Q_{3-\mu}^{t}. \tag{3}$$

In this many-body Hamiltonian,

$$h_{\mathrm{ch.moy}}^{(\tau)} = h_{WS} + \Delta^{(\tau)}\left(P^{+^{(\tau)}} + P^{(\tau)}\right) - \lambda^{(\tau)} N^{(\tau)}$$

is the contribution of the mean field which describes on one hand the quantized single particle motion of protons ($\tau = -1$) and neutrons ($\tau = +1$) in a Woods-Saxon potential and, on the other hand, pair correlations induced by a monopole pairing potential that related to the pair gap $\Delta^{(\tau)}$ and the pair operator $P^{+^{(\tau)}} = \sum_\gamma a_{\gamma+}^{(\tau)^+} a_{\gamma-}^{(\tau)^+}$ for protons and neutrons, correspondingly. The use of the Woods-Saxon potential is an improvement of the approach described in Ref. [38].

The additional term $\lambda^{(\tau)} N^{(\tau)}$ permits to fix the particle numbers (Z, N) with the help of the Fermi energy $\lambda^{(\tau)}$, Actually, the gap parameters $\Delta^{(p.n)}$ are calculated using the mass differences between odd and even nuclei.

The other terms of the Hamiltonian are the two two-body residual interaction which includes the isoscalar ($t = 0$) and isovector ($t = 1$) dipole-dipole ($\lambda = 1$) and octupole-octupole ($\lambda = 3$) interaction terms. The multipole operators $Q_{\lambda\mu}^{t}$ are defined by the combinations $Q_{\lambda\mu}^{t} = \left[r^\lambda Y_{\lambda\mu}\right]^{\mathrm{proton}} + (-1)^t \left[r^\lambda Y_{\lambda\mu}\right]^{\mathrm{neutron}}$ and the constants $\chi_{\lambda\mu}^{t}$ determine the strength of the corresponding multipole coupling. Possible terms associated to the quadrupole-quadrupole interaction are not taken into account because they describe positive parity quadrupole ($E2$) transitions that are weakly excited by photons below 20 MeV.

Applying the QRPA on the above Hamiltonian H_{E1}^{QRPA}, we will construct the possible vibrational modes excited via an $E1$ photo reaction.

The first step of the QRPA calculations diagonalises the mean field part $h_{\mathrm{ch.moy}}^{(\tau)}$.

.

4.1.1. **Diagonalisation of the mean field hamiltonian**

The residual interaction is neglected in the first step and the Hamiltonian associated to the proton and neutron system is separately diagonalised using a harmonic oscillator basis. Subsequently, a BCS transformation is performed. As a result of these diagonalisations, the particle operators (a_i^+, a_i) become transformed to quasi-particle operators (α_i^+, α_i). The mean field hamiltonian gets in this representation the diagonalised form $h_{\mathrm{ch.moy}}^{(\tau)} = \sum_i E_i^{(\tau)} (\alpha_i^+, \alpha_i)^{(\tau)}$ where $E_i^{(\tau)}$ is the quasi-particle energy of protons and neutrons, respectively .

4.1.2. **The equation of motion (EoM) of the QRPA and its solution**

Now the residual interaction terms of the Hamiltonian $H_{E1}^{\rm QRPA}$ must be taken into account. We give here only a brief sketch of the QRPA procedure in which the so-called quasi-boson approximation is an essential step to achieve the diagonalisation of the complete Hamiltonian $H_{E1}^{\rm QRPA}$. When expressing the multipole operator $Q^{(\tau)} = \sum_{kk'} q_{kk'} a_k^+ a_{k'}$ in terms of quasi-particle operators (α_i^+, α_j), one obtains sums implying pair operator terms like α_i^+, α_j^+, α_i, α_j and α_i^+, α_j. The first two of these pairs have approximately commutation relations like bosons such that one can write $\alpha_i^+, \alpha_j^+ \approx b_{ij}^+$ and $\alpha_j, \alpha_i \approx b_{ij}$, but now b_{ij}^+ and b_{ij} mean boson operators. With this quasi-boson approximation the multipole operator reads as

$$Q^{(\tau)} = \sum_{ij} \left[F_{ij}^{(\tau)} b_{ij}^+ + F_{ij}^{'(\tau)} b_{ij} \right] , \tag{4}$$

where $F_{ij}^{(\tau)}$ and $F_{ij}^{'(\tau)}$ are constants. The advantage of the boson representation (4) is that it is obviously linearly dependent on the boson operators (b_{ij}^+, b_{ij}), whereas it depends quadratically in terms of the fermion operators α_i^+, α_j. Expressing the mean field part of the total Hamiltonian in terms of bosons, one has

$$h^{(\tau)} = \sum_{ij} E_{ij}^{(\tau)} (b_{ij}^+ b_{ij})^{(\tau)}, \tag{5}$$

where $E_{ij} = E_i + E_j$ are the two-quasiparticle energies which play a crucial role for the formation of collective $E1$ excitations. According to Eq. (4), the residual interaction, schematically written as $Q^{(\tau)} Q^{(\tau)}$, gets now a quadratical form in terms of bosons. Hence, by using Eq. (3), we can write down the EoM for the vibrational modes (n) as

$$\left[H_{E1}^{\rm QRPA}, O_n^+ \right] = \hbar\omega_n O_n^+ , \tag{6}$$

where $O_n^+ = \sum_{kk'} \left(\phi_{kk'}^n b_{kk'}^+ - \psi_{kk'}^n b_{kk'} \right)$ is the excitation operator of a vibrational phonon with excitation energy $\hbar\omega_n$. The evaluation of the EoM (6) results in a matrix diagonalisation which leads to the eigenvalues $\hbar\omega_n$ and the QRPA amplitudes $\phi_{kk'}^n$ and $\psi_{kk'}^n$. The isovector coupling constant was parametrized as $\chi_{t=1} = (m\omega_0^2/A)\eta$ [39]. The factor η was chosen so as to reproduce the energy position of the GDR.

For the isoscalar multipole coupling constant, a high value $(\chi_{t=0} \geq 100\,\chi_{t=1})$ was taken in order to remove effects from the center of mass motions which may give spurious contributions to the calculated cross section [40]. With this choice, one can insert directly the full proton charge for the calculation of the $E1$ transition strength, thus avoiding the use effective charges for proton and neutron.

The $E1$ transition probability of a selected QRPA excitation at energy $\hbar\omega_n$ is given by

$$B_n(E_1) = \frac{1}{3} \sum_{\mu=0,\pm1} \left| \langle 0|O_n M(E1,\mu)|0\rangle \right|^2 \tag{7}$$

where $|0\rangle$ is the QRPA vacuum state and $M(E1,\mu) = e^{(p)} r Y^1_{\mu=0,\pm1}$ is the operator associated to the dipole moment.

The photo absorption cross section, σ_γ, is then calculated as

$$\sigma_\gamma(E1, E_x = \hbar\omega_n) = \frac{16\pi^3}{3\hbar c} E_x B_n \left(E1, \frac{1}{2}^{-1} \to \frac{1}{2}^{+1}, \frac{3}{2}^{+1} \right). \tag{8}$$

4.2. QRPA results and comparison to experiment

The photo absorption cross sections $\sigma_\gamma(E1, E_x)$ calculated with the QRPA solutions ($E_n = \hbar\omega_n$) form a spectrum of discrete lines. They can not be compared directly to the experimental values which are a continuous function for energies higher than the threshold. For this reason, the following treatment is made before the comparison. Every line E_n in the spectrum with a QRPA cross section value $\sigma_\gamma(E1, E_x)$ is convoluted with a Breit-Wigner function $f_n(E_x, \Gamma)$ of the form

$$\sigma_\gamma(E1, E_x) \frac{\Gamma}{2\pi\left[(E_x - E_n)^2 + \Gamma^2\right]}. \tag{9}$$

E_x is the excitation energy, E_n is the energy of the line and Γ is the parameter broadening of the Lorentzian obtained by interpolation in such a way that the maximum position of the GDR is reproduced.

The total spectrum QRPA is then obtained by the summation

$$\sigma_\gamma(E1, E_x) = \sum_n \sigma_\gamma(E1, E_n) \frac{\Gamma}{2\pi\left[(E_x - E_n)^2 + \Gamma^2\right]}. \tag{10}$$

Figure 12 represents the QRPA photo absorption cross section for $E1$ transitions compared to the experimental ones. Both, the experimental as well as the calculated cross section can not distinguish between the partial cross sections of the $E1$ transitions $\frac{1}{2}^{-1} \to \frac{1}{2}^{+1}$ and $\frac{1}{2}^{-1} \to \frac{3}{2}^{+1}$, respectively.

The general behaviour is well reproduced which consolidates the hypothesis of vibrational excitations generated by collective two-quasiparticle (two-quasihole) character. Particularly, in the energy region between 6 and 11 MeV, the QRPA model gives account on the enhancement of the transition probabilities below 12 MeV which can not be described by the tail of a Lorentzian curve.

QRPA calculations in the neighboring isotones ^{88}Sr and ^{90}Zr give the same findings. The comparison shows that the unpaired proton in ^{89}Y plays no significant role.

Calculations in ^{90}Zr using the quasi-photon model [22] show that this enhancement is due to oscillations of the excessive neutrons against a $N = Z$ neutron proton core which is usually called PDR. It will be good in the future to explore this excitation mode in nuclei far from stability with proton excess.

5. *Summary*

We have performed photon scattering experiments on ^{89}Y using the bremsstrahlung facility at the ELBE accelerator up to the giant dipole resonance. Comparing the spectra obtained at different electron energies, about 250 levels were identified. Using GEANT3 simulations, the background corresponding to atomic processes in the detectors and in the target was subtracted from the spectra which include resolved and unresolved (continuum) transitions. Then the intensity distribution was corrected for the branching transitions by using simulations of gamma ray cascades based on the BSFG model and statistical fluctuations of the partial widths. A comparison of the photoabsorption cross section obtained in this way from the present experiment with (γ, n) data shows a smooth connection of the two data sets and gives new information about the extension of the GDR toward lower energy. In this extension, a small resonance compared to the GDR appears in the energy range from 6 to 11 MeV formed from extra $E1$ strength. QRPA calculations are in qualitative agreement with this finding.

References

[1] U. Kneissl et al., Prog. Part. Nucl. Phys. **37** (1996) 349.

[2] F. Iachello, Phys. Lett. B **160** (1985) 1.

[3] R. D. Herzberg et al., Nucl. Phys. A **592** (1995) 211.

[4] N. Ryezayeva et al., Phys. Rev. Lett. **89** (2002) 272502.

[5] R. Schwengner et al., Phys. Rev. C **81** (2010) 054315.

[6] N. Pietralla et al., Phys. Rev. Lett. **88** (2001) 012502.

[7] S. Volz et al., Nucl. Phys. A **779** (2006) 1.

[8] K. Govaert et al., Phys. Rev. C **57** (1998) 2229.

[9] A. Zilges et al., Phys. Lett. B **542** (2002) 43.

[10] T. Hartmann et al., Phys Rev Lett. **93** (2004) 192501.

[11] Y. Suzuki et al., Prog. Theor. Phys. **83** (1990) 180.

[12] J. Chambers et al., Phys. Rev. C **50** (1994) R2671.

[13] J. P. Adams et al., Phys. Rev. C **53** (1996) 1016.

[14] D. Sarchi et al., Phys. Lett. B **601** (2004) 27.

[15] J. Piekarewicz et al., Phys. Rev. C **73** (2006) 044325.

[16] N. Paar et al., Phys. Lett. B **606** (2005) 288.

[17] N. Tsoneva et al., Phys. Rev. C **77** (2008) 024321.

[18] P. G. Hansen et al., Ann. Rev. Nucl. Part. Sci. **45** (1995) 591.
[19] E. Tryggestad et al., Phys. Lett. B **541** (2002) 52.
[20] K. Langanke, Rep. Prog. Phys. **64** (2001) 1657.
[21] G. Rusev, dissertation, Technische Universität Dresden, 2007.
[22] R. Schwengner et al., Phys. Rev. C **76** (2007) 034321.
[23] R. Schwengner et al., Phys. Rev. C **78** (2008) 064314.
[24] N. Benouaret et al., Phys. Rev. C **79** (2009) 014303.
[25] UEP. Berg et al., Ann. Rev. Nucl. Part. Sci. **37** (1987) 33.
[26] U. Kneissl et al., Prog. Part. Nucl. Phys. 37349??? (1996)
[27] R. Schwengner et al., Nucl. Instrum. Methods A **555** (2005) 211.
[28] CERN Program Library Long Writeup W5013, Geneva, 1993 (unpublished).
[29] E. Haug, Radiat. Phys. Chem. **77** (2008) 207.
[30] J. Reif et al., Nucl. Phys. A **620** (1997) 1.
[31] T. von Egidy et al., Phys. Rev. C **72** (2005) 044311.
[32] T. A. Brody et al., Rev. Mod. Phys. **53** (1981) 385.
[33] C. E. Porter and R. G. Thomas, Phys. Rev. **104** (1956) 483.
[34] P. Axel, Phys. Rev. **126** (1962) 671.
[35] A. Lepretre et al., Nucl. Phys. A **175** (1971) 609; http://wwwnds.iaea.org/exfor/.
[36] A. J. Koning et al., AIP Conf. Proc. **769** (2005) 1154.
[37] P. Ring and P. Schuck, *The Nuclear Many Body Problem*, Springer-Verlag, Berlin, Heidelberg (1980).
[38] D. J. Rowe, *Nuclear Collective Motion*, Methuen, London (1970).
[39] F. Dönau et al., Phys. Rev. C **76** (2007) 014317.
[40] F. Dönau et al., Phys. Rev. Lett. **94** (2005) 092503.

ISTRAŽIVANJE DIPOLNIH UZBUDA U ^{89}Y ISPOD GIGANTSKE DIPOLNE REZONANCIJE U POGONU ELBE

Istraživali smo dipolne rezonancije u stabilnoj jezgri ^{89}Y s $N = 50$ do energije uzbude giganske dipolne rezonancije (GDR) rabeći sustav za kočno zračenje pri ubrzivaču ELBE u istraživačkom središtu Dresden-Rosendorf. Nakon uklanjanja pozadinskog zračenja od atomskih procesa kao i od neelastičnih prijelaza u spektrima, mogli smo, primjenom statističkih metoda, odrediti fotoapsorpcijske udarne presjeke za podatke o fotonskom raspršenju. Ti su udarni presjeci povezani s onima iz mjerenja (γ, n) reakcija. Našli smo višak u udarnim presjecima u odnosu na jednostavno Lorentzovo približenje u repu GDR, u području energije od oko 6 MeV do 11 MeV. Usporedba s približenjem kvazičestica i slučajnih faza pokazuje na mogućnost da su odgovorne uzbude uzrokovane oscilacijama viška neutrona koji načine tzv. "pigmy" dipolnu rezonanciju, nađenu u susjednim izotonima ^{88}Sr i ^{90}Zr.